IJARST

International Journal of Advanced Research in Science and Technology

https://doi.org/10.62226/ijarst2024132542

ISSN 2319 – 1783 (Print)
ISSN 2320 – 1126 (Online)

Integration of Slots and Complementary Split Ring Resonators (CSRRs) for High-Gain Dual-Band Compact Microstrip Patch Antennas for 5G Applications

M. A. YUSUF[1,*] and M. H. ALI[2]

[1]Department of Physics, Abubakar Tafawa Balewa University, Bauchi.

[2]Department of Physics, Bayero University, Kano.

[1]yamuhammad@atbu.edu.ng, [2]mhali.phy@buk.edu.ng

ARTICLEINFO

Article history:

Received	15 Apr 2025
Accepted	23 Apr 2025
Available online	24 May 2025

Keywords:

5G,
Antenna Bandwidth,
CSRRs,
Gain,
Micro strip Antennas,
Slots

ABSTRACT

This paper presents the integration slots and Complementary Split Ring Resonators (CSRRs) in the development of miniaturized, high-gain, dual-band Microstrip Rectangular Patch Antennas (MRPAs) for 5G mobile communication applications. The antennas were designed on a Rogers RT5880 substrate with a thickness of 0.508 mm. Slots and CSRR metamaterial unit cells were integrated into the patch and ground planes, respectively, to achieve size reduction, high gain, and bandwidth enhancement. The design and simulation processes were conducted using CST Studio Suite 2018. Simulated results of the best-performing antenna showed that integrating CSRRs reduces the MRPA size by approximately 25%, from 330 mm² (16.5 × 20.0 mm²) to 248 mm² (15.5 × 16.0 mm²). The conventional MRPA antenna without slots and CSRRs resonated at 26.59 GHz and 28.0 GHz, offering bandwidths of 0.50 GHz and 0.81 GHz, with corresponding gains of 5.81 dB and 9.44 dB, respectively. After integrating the slots and CSRRs, the MRPA antenna resonated at 26.75 GHz and 28.0 GHz, with bandwidths increased to 0.52 GHz and 1.10 GHz (enhancements of 4% and 36%), and gains improved to 9.20 dB and 11.39 dB (enhancements of 58% and 21%), respectively. These enhancements and size reduction make the proposed slotted and CSRR-loaded MRPA antennas suitable for millimeter-wave 5G wireless portable devices.

1.0 INTRODUCTION

Over the past four decades, network communication has advanced from 1G analog systems to 5G mm-wave technology to meet rising wireless demands [1]. The application of 5G is motivated by the demand for faster data rates and low latency communication, supporting growing mobile traffic from streaming, social media, and data centers [2]-[3]. Recognizing the need for high-speed wireless communication, Countries worldwide are rapidly accepting 5G infrastructure to handle growing mobile device usage, ensuring ultra-fast transmission, expanded capacity, and energy-efficient networks for smart cities, virtual reality, and autonomous vehicles [4]-[5]. Microstrip Patch Antennas (MPAs) have emerged as capable candidates to meet these demands and are gradually integrated into 5G mobile communication systems, as confirmed by recent studies [6].

MPA antennas, valued for their discrete design, compact size, portability, cost-effectiveness, and compatibility with integrated circuit technology, play a crucial role in numerous wireless communication systems, including GPS, RFID, and cell phones [7]. As technology advances, particularly with the advent of 5G applications, researchers are increasingly concentrating on enhancing MPA radiation characteristics to satisfy the demands of contemporary communication systems [8]. This enhancement is often achieved through slots, CSRRs, microstrip patch arrays, etc. Introducing slots in the patch reduces the patch size, improves bandwidth, and helps control the radiation pattern [9]. CSRRs are commonly used to attain left-handed meta material properties (reduce the effective permittivity and permeability), which leads to antenna miniaturization, enhancing bandwidth, and improving the antenna's impedance matching [10]. Arrays offer superior performance in beam steering, bandwidth, gain, directivity, and flexibility to meet precise application requirements, so they are widely preferred in many radar and communication systems.

However, despite the superior bandwidth and gain characteristics of micro strip patch arrays, their larger size, increased weight, and complexity make them less practical for many applications, particularly in portable devices such as smartphones, tablets, and laptops. Consequently, significant research efforts in the

literature focus on addressing these challenges through two fundamental approaches: integrating slots and employing CSRRs.

In [11], a CSRR-loaded T-shaped MIMO antenna with a gain of 6.4 dB at 28 GHz was fabricated for 5G vehicular and cellular communications on a 12x25.4x0.8 mm^3 Rogers RT substrate. In [12] a rectangular-shaped slotted MPA using a microstrip feeding technique was presented. It resonates at 27.97 GHz, featuring an S_{ll} of -20.95 dB, a bandwidth of 1.06 GHz, a gain of 7.5 dB, and an efficiency of 99.83%. Similarly, [13] analyzed an MPA for future application in 5G at 28 GHz, reporting an S_{11} of -38.348 dB, a gain of 8.198 dB, a VSWR of 1.02, and an efficiency of 77%. In [1] a 15x15x1.52 mm^3 high-gain CSRR-loaded MIMO patch antenna for wireless 5G devices was explored, achieving a realized gain of 8.65dB at 28 GHz and 8.24 dB at 38 GHz. Furthermore, [14] uses an artificial neural network to design a CSRR-inspired MPA for 5G devices at sub-6 GHz. Constructed on an FR4 substrate of 28 × 28 × 1.6 mm^3, the integration of metamaterials on the radiator enabled dual-band operation at 3.6 GHz and 5.2 GHz, achieving gains of 5.75 dB and 6.3 dB, bandwidths of 0.7 GHz and 1.04 GHz, and efficiencies of 93.9% and 91.8%, respectively. As the demand for compact hand-held devices rises, miniaturized MPAs with wide bandwidth and high gain are crucial for seamless integration into 5G applications, eliminating the need for arrays.

This work explored the integration of slots and CSRRs to miniaturize an MRPA antenna while addressing its intrinsic challenges of narrow bandwidth and low gain in the 26 GHz and 28 GHz mm-wave 5G bands. The objective is to significantly enhance the antenna's bandwidth and gain while maintaining a compact and lightweight design. This is achieved by integrating slots in the patch and CSRRs into the ground plane.

2.0 BACKGROUND THEORY

This section introduces the theoretical equations for integrating the patch's effective area and the CSRRs into a single microstrip patch antenna design.

2.1 Effective area of patch antenna

The effective area and dielectric material of a microstrip patch antenna are crucial in determining its gain, radiation pattern, efficiency, and overall performance in transmitting and receiving electromagnetic signals [15]. Precise design of the effective area is essential for achieving optimal performance, particularly in advanced communication systems like 5G [16].

The beam area or beam solid angle Ω_A for an antenna is given by the integral of the stabilized power pattern over a sphere

$$\Omega_A = \int_0^{2\pi}\int_0^{\pi} P_n(\theta,\emptyset)d\Omega \quad (1)$$

Directivity (D) is calculated from:

$$D = \frac{4\pi}{\Omega_A} \quad (2)$$

where Ω_A = beam solid angle

The lower the beam's solid angle, the higher the directivity.

Also, the antenna Gain (G) is given by:

$$G = kD \quad (3)$$

where k is the efficiency factor of the antenna and D is the directivity given in equation (2) [15].

In MPA antenna design, selecting the dielectric substrate, substrate thickness, and resonant frequency is critical. These selections determine key parameters such as patch dimensions and feed location, which can be calculated using equations (4-9) [6].

For instance, the width of the patch (W_p) can be written as:

$$W_p = \frac{c}{2f_o}\sqrt{\frac{2}{\varepsilon_r+1}} \quad (4)$$

where c signifies the speed of an electromagnetic wave in a vacuum, f_o refers to the resonant frequency, and $\varepsilon_r$denotes the substrate's relative dielectric value.

The fields at the patch edges exhibit fringing due to the patch's finite dimensions. This fringing effect makes the patch appear electrically larger than its physical dimensions. Equation (5) establishes a relationship between the patch's effective patch length (L_{eff}) and its actual physical length (L_p), which takes into consideration the length extension (△L) at each end. Equation (6) shows how the effective dielectric constant (ε_{reff}), which accounts for fringing and wave propagation effects, influences both the actual length of the patch and the extension of that length [17].

$$L_{eff} = L_p + 2\Delta L = \frac{c}{2f_0\sqrt{\varepsilon_{reff}}} \quad (5)$$

where the effective dielectric constant (ε_{reff}), and the length variation (ΔL) are defined as:

$$\varepsilon_{reff} = \frac{\varepsilon_r+1}{2} + \frac{\varepsilon_r-1}{2}\left[1+12\frac{h}{W_p}\right]^{-1/2} \quad (6)$$

$$\Delta L = 0.412h\left[\frac{(\varepsilon_{reff}+0.3)\left(\frac{W_p}{h}+0.264\right)}{(\varepsilon_{reff}-0.258)\left(\frac{W_p}{h}+0.8\right)}\right] \quad (7)$$

while the length of the substrate (L_s) is given by:

$$L_s = 6h + L_p \quad (8)$$

and finally, the width of the substrate (W_s) is given by:

$$W_s = 6h + W_p \quad (9)$$

where h represents the thickness of the dielectric substrate

2.1 Split Ring Resonators (SRRs) and Complementary Split Ring Resonators (CSRRs)

Amongst the diverse left-handed materials (LHMs), Split Ring Resonators (SRRs) are meta material structures that produce negative permeability (-μ) when activated by an axial magnetic field. Due to its high conductivity, the capacitance between the rings compensates for the inductance in the SRRs [18]. Plate 2 demonstrates the two most popular SRRs and CSRRs configurations, along with the equivalent circuit models. The SRRs are made up of conductive wire loops that function as inductors and small open gaps that function as capacitors, as shown in Plate 2(a). In contrast, the CSRRs are formed by engraving the negative pattern of the SRRs onto the ground plane, as depicted in Plate 2(b).

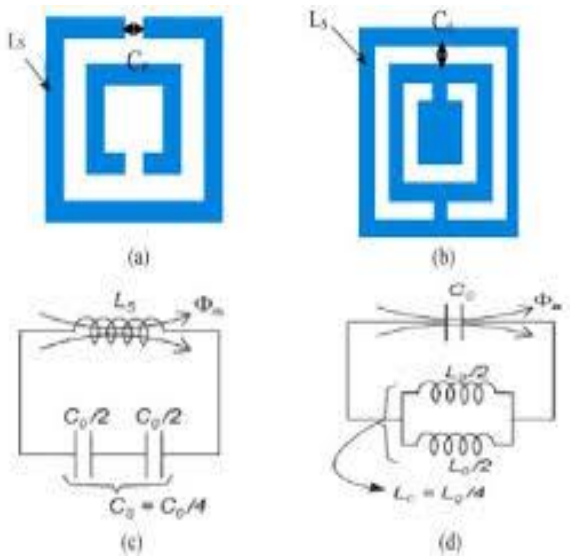

Plate 2. Configurations of square (a) SRRs, (b) CSRRs, and (c-d) their respective circuit models [18].

Both structures operate as *LC* resonators based on the analysis of SRRs and CSRRs. In the equivalent circuit model of Plate 2(c), the SRR's inductance *Ls* is changed by the capacitance Cc in Plate 2(d), which encircles the ground plane. Moreover, the two series-connected capacitances in Plate 2(c) are substituted by two parallel-connected inductances in Plate 2(d), establishing a connection between the innermost disk and the ground.

Designing square CSRRs for an MPA antenna involves careful consideration of the dimensions of the outside and inside square rings, their widths, and the spacing between them. These factors are crucial for attaining the desired resonant frequency, illustrated in equation (10) [19]-[20].

$$f_r = \frac{1}{2\pi\sqrt{L_s C_s}} \qquad (10)$$

The rings and slit introduce capacitance and inductance, forming an LC circuit used to determine the operating frequency. Equations (11) to (15) were applied to compute the CSRR frequencies.

where,

$$L_s = \frac{\mu_o}{2}\frac{L_{avg}}{4} 4.86 \left[\ln\frac{0.98}{\rho} + 1.84\rho\right] \qquad (11)$$

$$L_{avg} = 4[L_s - (N-1)(w+s)], \qquad (12)$$

$$\rho = \frac{(N-1)(w+s)}{[L_s-(N-1)(w+s)]} \qquad (13)$$

$$C_s = \varepsilon_o \frac{N-1}{2}\left[2L_s - (2N-1)(w+s)\frac{K\sqrt{1-k_1^2}}{K(k_1)}\right] \qquad (14)$$

where N is the number of CSRR Rings, L_s is the CSRR's Length, w is the CSRR's width, L_{avg}= The square SRR/CSRR average length, ρ = filling ratio, k = First kind complete elliptic integral, k_1= The integral argument, which is stated as:

$$k_1 = \frac{S/2}{W+S/2} \text{ [18].} \qquad (15)$$

It can be seen from equations (11) through (15) that the inductance due to the dimensions of the outer square ring, inner square ring, the width of the rings, and the capacitance due to the gap between the rings of CSRRs are crucial for achieving the desired resonant frequency for better performance. Therefore, the area, dA and the dielectric permittivity of a single patch antenna can be modified using slots and CSRRs in a CST simulation environment to obtain the optimum value for a given frequency band before fabrication, securing more space normally occupied by the array.

3.0 MATERIALS AND METHODS

3.1 Materials

Since this research is purely simulation-based, we used CST Studio Suite 2018 simulation software, its virtual copper, and Rogers RT5880 substrate.

3.2 Antenna Design

This study adopts a design approach focused on rectangular patch antennas, similar to those by [1,9,21]. The antenna in Figure 2(a-b) was developed on a Rogers RT5880 substrate that measured 16.5 × 20 × 0.508 mm^3, had a relative dielectric permittivity (εr) of 2.2, and a tan δ of 0.0009. Then, an inset feeding method was employed to realize optimal impedance matching amid the patch and the feeding line, as it's a preferred method in MPAs [9]. The rectangular patch, measuring 10.2 × 10.8 × 0.035 mm3, was then fed via a 4.85 mm-long and 0.7 mm-wide feed line.

Figure 3(a-c) presents the slots and CSRR-loaded MRPA, designed on a 15.5 × 17 × 0.508 mm^3 Rogers RT5880 substrate with a rectangular patch measuring 9.8 × 10.0 × 0.035 mm^3, fed by a 4.2 mm length and 0.7 mm wide microstrip feed line. Figure 4 and Figure 5 present patches of 9.72 × 9.9 × 0.035 mm^3 and 9.73 × 9.9 × 0.035 mm^3, respectively, both designed on 15.5 x 16 x 0.508 mm^3 substrates, fed by 4.25 mm length and 0.7 mm wide feed lines. Lastly, to reduce the antenna's

size, increase its range of usable frequency, and gain performance, slots and CSRRs were etched into the Table l presents the measurements of the conventional MRPA depicted in Figures 2(a-b). Tables 2, 3, and 4 present the measurements of the LIU, LIL, and LI□ patch and ground layers of the antennas, respectively.

shaped slots and CSRR-loaded MRPAs depicted in Figures 3(a-c), 4(a-c), and 5(a-c), respectively.

Table l: Measurements of the inset-fed conventional MRPA antenna (in millimeters)

Parameter	Ls = Lg	Ws = Wg	L_p	W_p	L_f	W_f	Y_O	X_O
Dimension	16.5	20.0	10.2	10.8	4.85	0.7	0.65	0.55

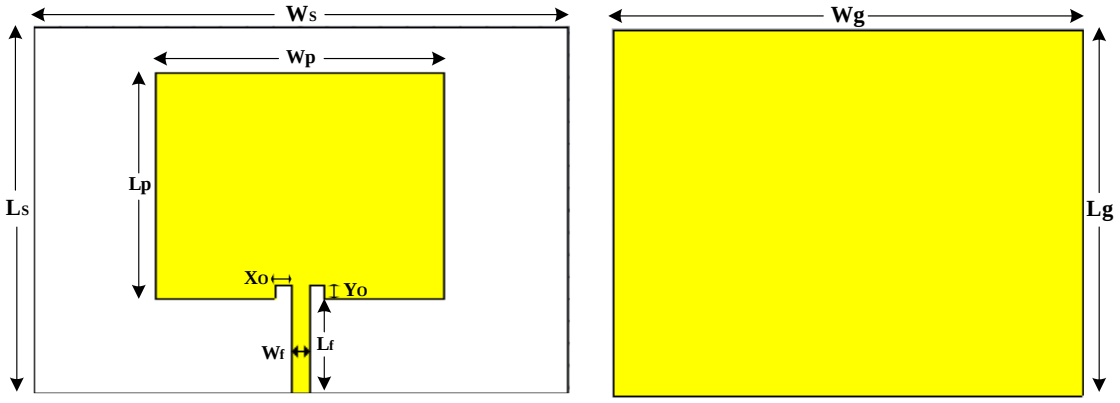

(a) Front perspective (b) Back perspective

Figure 2(a-b): The design geometry of the front and back perspectives of conventional MRPA

Table 2: Measurements of the inset-fed LIU slotted CSRR-loaded MRPA antenna (in millimeters)

Parameter	Ls=Lg	Ws=Wg	L_p	W_p	L_f	W_f	RA	RW_1	RW_2	S	W	G
Dimension	15.5	17.0	9.8	10.0	4.2	0.7	8.05	1.3	1.0	0.1	0.1	0.5

Parameter	SL_I	SW_I	SL_2	SW_2	SL_3	SW_3	SL_4	SW_4	SL_5	SW_5	Y_O	X_O
Dimension	0.75	1.75	5.05	0.75	4.90	0.85	1.00	3.70	2.45	1.20	2.20	0.70

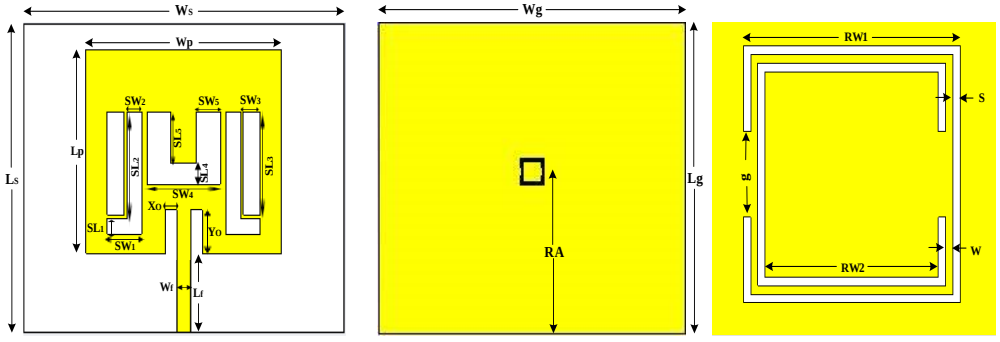

(a) Front perspective (b) Back perspective with CSRRs (c) CSRRs

Figure **3(a-c)**: The geometric design of the LIU-shape slotted MRPA loaded with CSRRs structure

Table 3: Measurements of the inset-fed LIL slotted CSRR-loaded MRPA antenna (in millimeters)

Parameter	Ls=Lg	Ws=Wg	L_p	W_p	L_f	W_f	RA	RW_1	RW_2	s	W	g
Dimension	15.5	16.0	9.72	9.9	4.25	0.70	8.25	1.30	1.00	0.10	0.10	0.50
Parameter	**SL_I**	**SW_I**	**SL_2**	**SW_2**	**SL_3**	**SW_3**	**SL_4**	**SW_4**	**SL_5**	**SW_5**	**Y_O**	**X_O**
Dimension	0.75	1.75	5.05	0.75	4.95	0.85	0.70	4.35	3.00	3.65	2.40	0.70

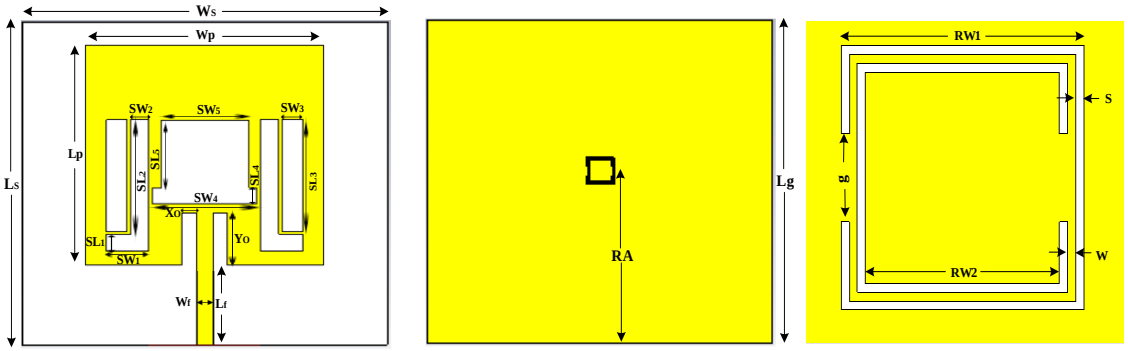

(a) Front perspective (b) Back perspective with CSRRs (c) CSRRs

Figure 4(a-c): The geometric design of the LIL-shape slotted MRPA loaded with CSRRs structure

Table 4: Measurements of the inset-fed LI□ slotted CSRR-loaded MRPA antenna (in millimeters)

Parameter	Ls=Lg	Ws=Wg	L_p	W_p	L_f	W_f	RA	RW_1	RW_2	s	w	g
Dimension	15.50	16.00	9.73	9.90	4.25	0.70	8.15	1.30	1.00	0.10	0.10	0.50
Parameter	**SL_I**	**SW_I**	**SL_2**	**SW_2**	**SL_3**	**SW_3**	**SL_4**	**SW_4**	**SL_5**	**SW_5**	**Y_O**	**X_O**
Dimension	0.75	1.75	5.20	0.75	5.05	0.85	4.00	4.20	-	-	2.40	0.70

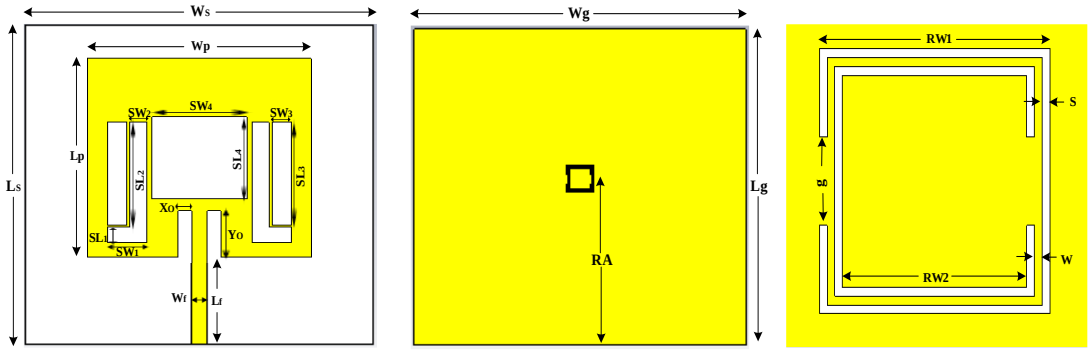

(a) Front perspective (b) Back perspective with CSRRs (c) CSRRs

Figure 5(a-c): The geometric design of the LI□ shape MRPA loaded with CSRRs structure

4.0 RESULTS AND DISCUSSION

The findings from the suggested conventional MRPA and the three different slotted CSRR-loaded MRPA antennas are provided in this section. Their performance is evaluated and compared based on size, bandwidth, and gain.

4.1 Performance of the designed conventional MRPA antenna

Table 5 shows the findings extracted from the antenna in Figure 2(a-b). The antenna exhibited good performance in the 28 GHz band regarding $S_{ll,}$ bandwidth, gain, and directivity. Similarly, the 26 GHz band exhibited good performance and high efficiency.

Table 5: Simulated results of the conventional MRPA antenna depicted in Figure 2(a-b)

Resonance Frequency (GHz)	Return loss S_{11} (dB)	Bandwidth (GHz)	VSWR	Gain (dB)	Directivity (dBi)	Efficiency (%)
26.59	-19.01	0.50	1.25	5.81	6.20	94.00
28.0	-34.57	0.81	1.04	9.44	10.40	91.00

However, to satisfy new 5G design specifications for mobile communication systems, the antenna size must be reduced while increasing bandwidth and gain. To achieve this, slots and CSRRs can be integrated into the patch and ground planes of the design, respectively. The S_{11} and bandwidth are shown in Figure 6(a), and the VSWR is shown in Figure 6(b). The gain and directivity at 26 GHz are displayed in Figures 7(a) and 7(b), whereas the gạin and directivity at 28 GHz are shown in Figures 8(a) and 8(b), respectively.

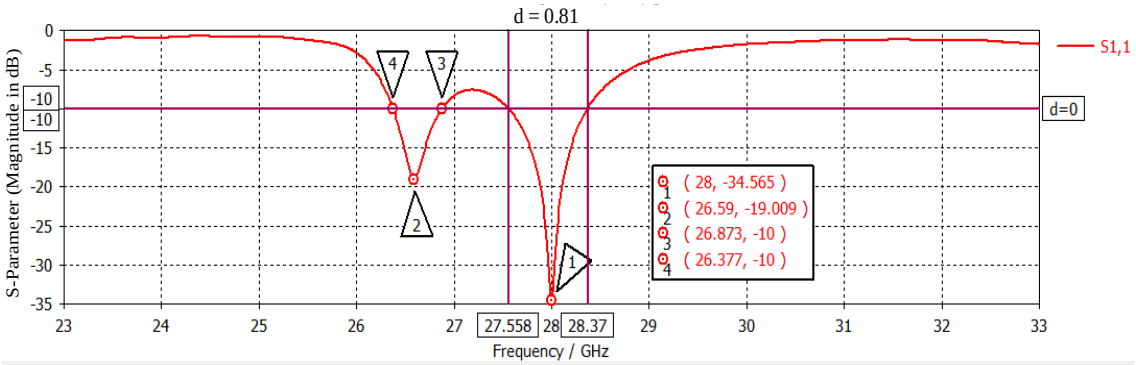

Figure 6(a): Return loss (S_{11}) and Bandwidth as frequency functions.

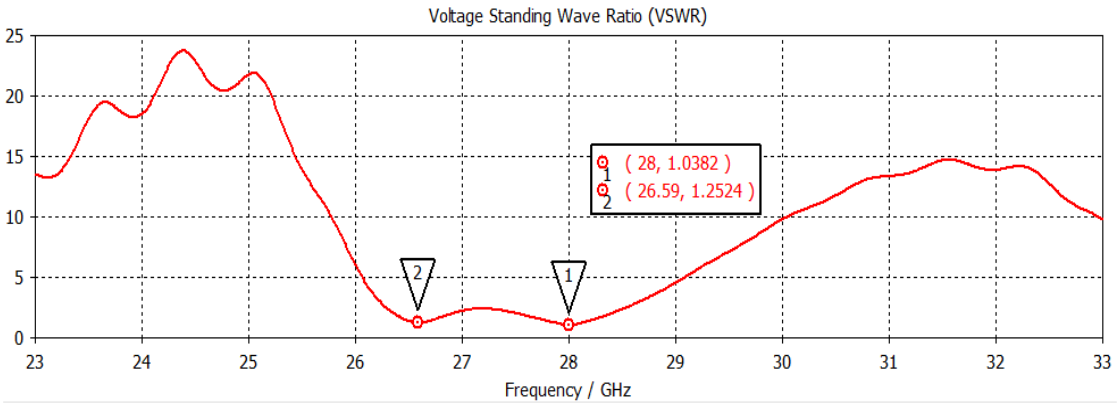

Figure 6(b): VSWR as a frequency function for the conventional MRPA antenna

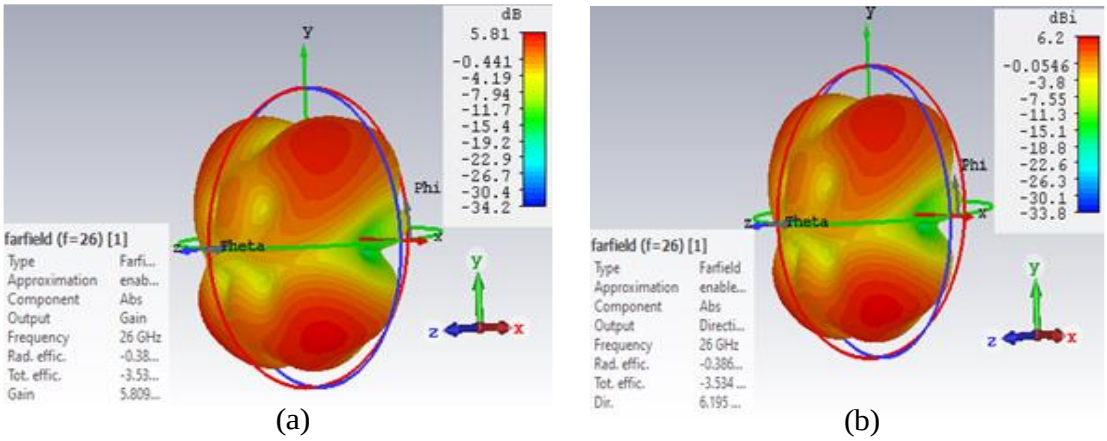

Figure 7(a)(b): Gain and directivity for the conventional MRPA antenna at 26 GHz

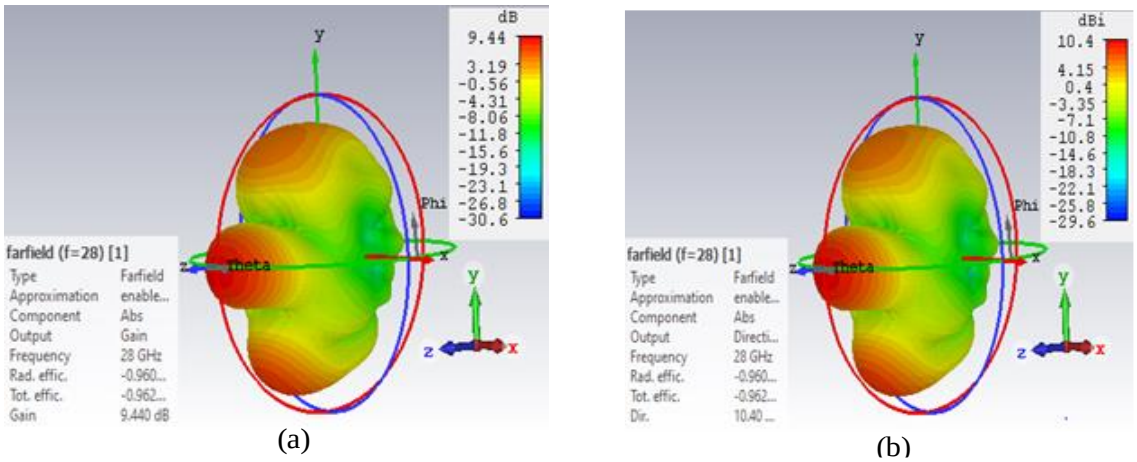

Figure 8(a)(b): Gain and directivity for the conventional MRPA antenna at 28 GHz

4.2 Performance of the LIU-shape slotted MRPA loaded with CSRRs structure

Miniaturization is crucial in MPA antenna design for 5G applications, but often compromises radiation performance. To address this issue, design 3(a-c) incorporates slots and CSRRs to minimize size while enhancing radiation performance. Table 6 presents performance outcomes derived from Figure 3(a-c). The antenna demonstrates strong performance, featuring a low S11 value, wide bandwidth, and high gain in the 28 GHz band. However, Figure 9(a) indicates that it fails to resonate at the 26 GHz band.

Table 6: Simulated results of the design depicted in Figure 2(a)

Resonance Frequency (GHz)	Return loss S_{11} (dB)	Bandwidth (GHz)	VSWR	Gain (dB)	Directivity (dBi)	Efficiency (%)
28.00	-30.37	1.16	1.06	9.95	11.07	90.00

However, enhancements may be necessary for gain, and efficiency to meet the emerging design requirements for 5G. This can be achieved by integrating various centrally positioned slot elements into the selected dual LI slots in the CSRR-loaded MRPA design. Figure 9(a) demonstrates the S_{11} and bandwidth; Figure 9(b) presents the VSWR, while Figures 10(a) and 10(b) illustrate the antenna gain and directivity at 28 GHz.

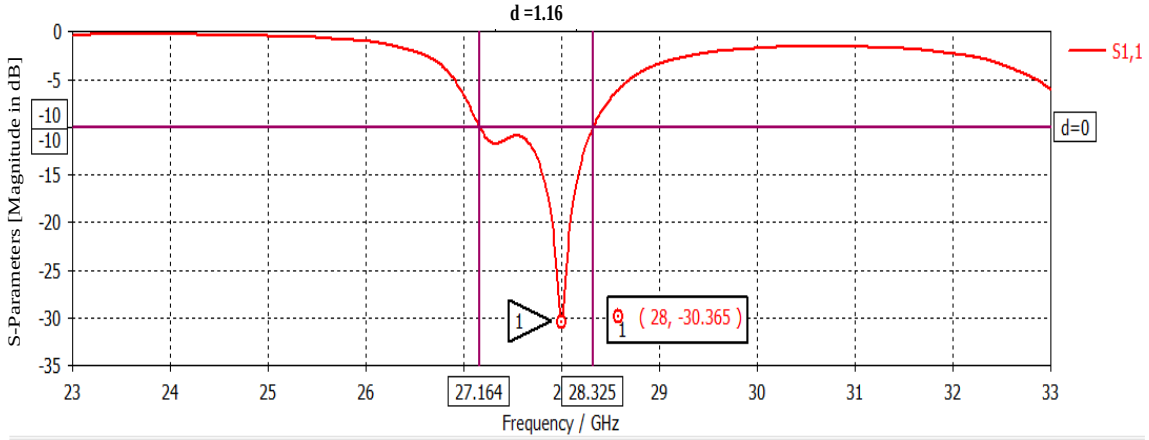

Figure 9(a): S_{11} and Bandwidth as functions of frequency for Design 3(a-c).

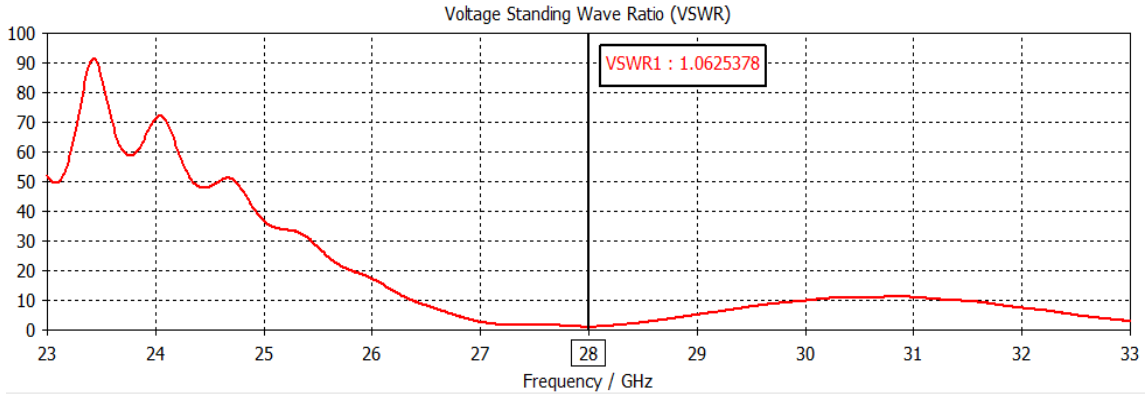

Figure 9(b): VSWR parameter as a function of frequency for Design 3(a-c)

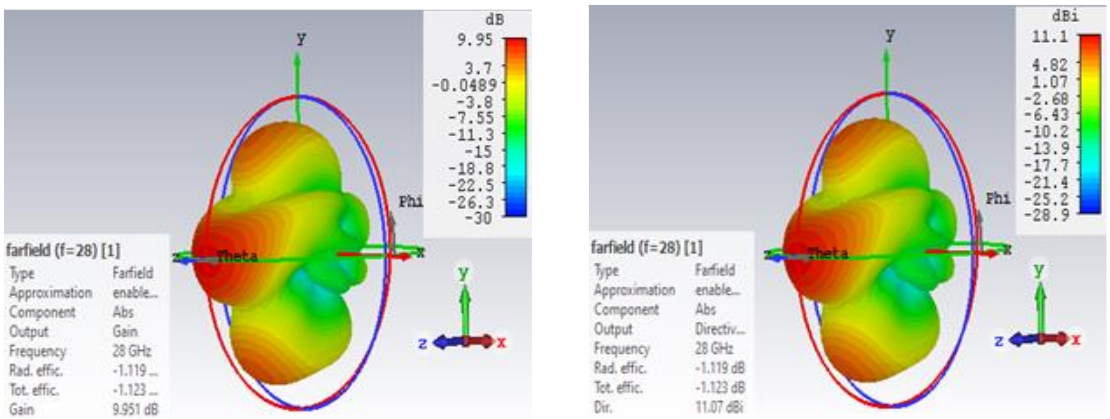

(a) (b)

Figures 10(a)(b): Simulated gain and directivity for the antenna design 3(a-c)

4.3 Performance of the LIL-shape slotted MRPA loaded with CSRRs structure.

From Table 7, the proposed antenna design in Figure 4(a-c) exhibits enhanced bandwidth, gain, directivity, and efficiency at 28 GHz, with high gain and efficiency observed at 26 GHz. Despite relatively narrow bandwidths at both frequencies, the design meets the necessities for mm-wave 5G applications. The S_{11} shown in Figure 11(a) remains well below –10 dB, signifying good impedance matching, as supported by the VSWR results in Figure 11(b). Figures 12(a) and 12(b) show the antenna gain and directivity at 26 GHz, while Figures 13(a) and 13(b) show the gain and directivity at 28 GHz, respectively.

Table 7: Simulated results of the design depicted in Figure 4(a-c)

Resonance Frequency (GHz)	**Return loss S_{11} (dB)**	**Bandwidth (GHz)**	**VSWR**	**Gain (dB)**	**Directivity (dBi)**	**Efficiency (%)**
26.23	-16.24	0.44	1.37	8.46	8.87	95.00
28.00	-30.66	0.95	1.06	11.19	11.96	94.00

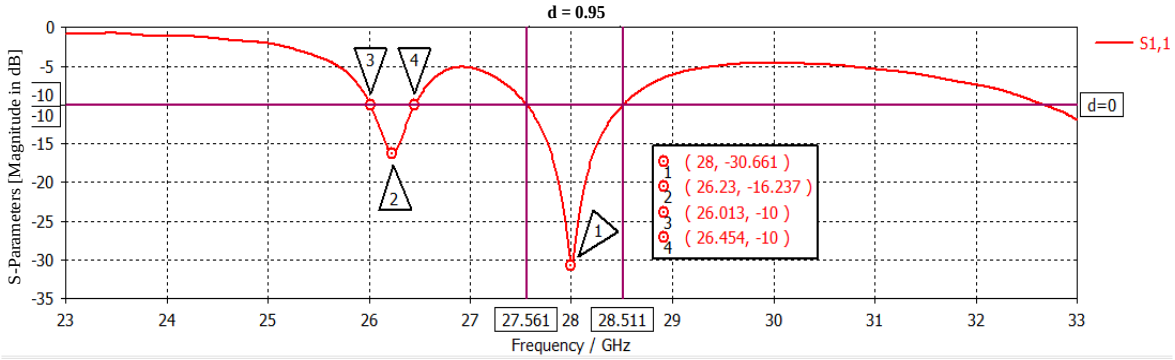

Figure 11(a): Return loss (S_{11}) and Bandwidth as functions of frequency

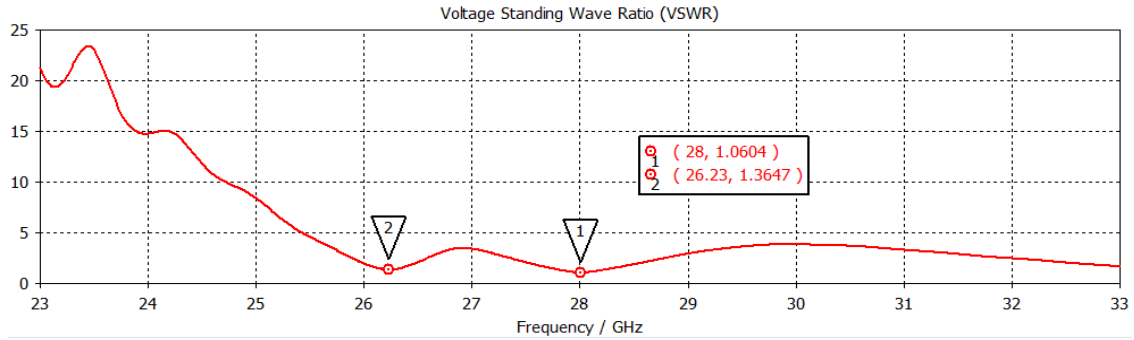

Figure 11(b): VSWR as a function of frequency for the antenna in Figure 4(a-c)

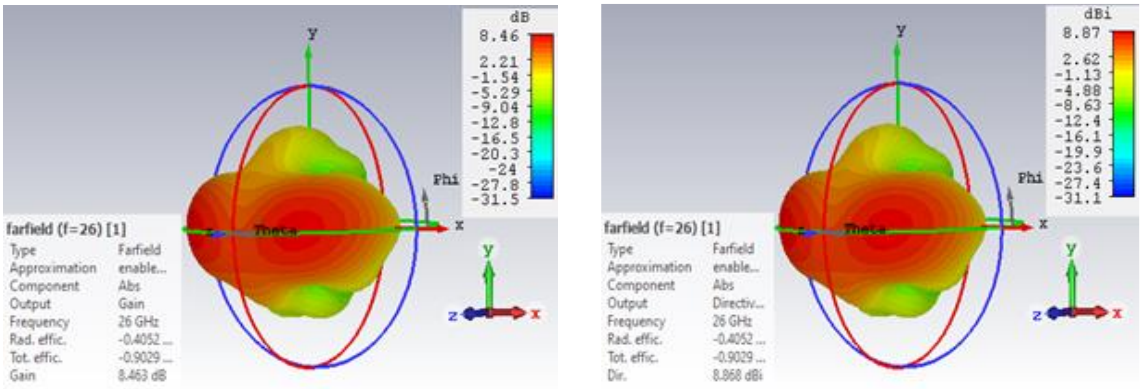

(a) (b)

Figure 12(a)(b): Simulated gain and directivity for the antenna in Figure 4(a-c) at 26 GHz

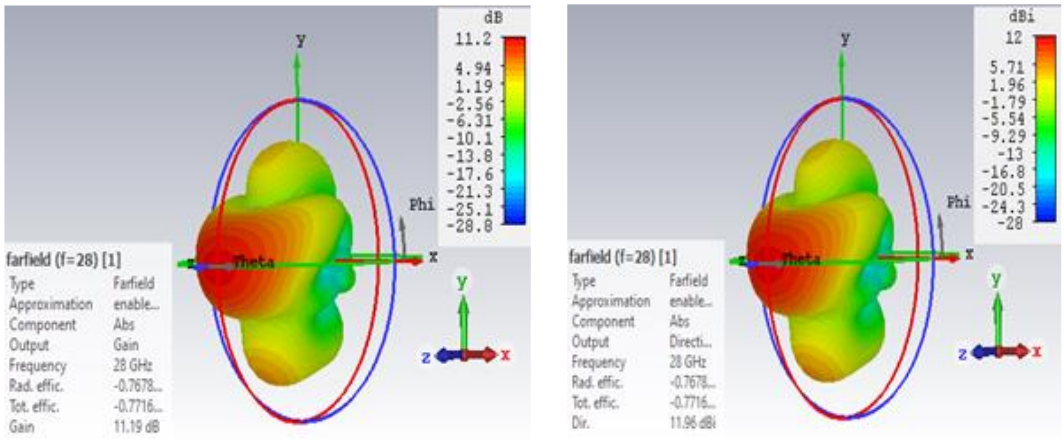

(a) (b)

Figure 13(a)(b) Simulated gain and directivity for the antenna in Figure 4(a-c) at 28 GHz

4.4 Performance of the LI□-shape slotted MRPA loaded with CSRRs structure.

According to the results in Table 8, the design enhanced radiation performance by increasing bandwidth, gain, and directivity at both frequency bands. Furthermore, efficiency remains high at 26 and 28 GHz despite the bandwidth, gain, and directivity enhancements.

Table 8: Simulated results of the CSRR-loaded MRPA antenna depicted in Figure 5(a-c)

Resonance Frequency (GHz)	Return loss S_{11} (dB)	Bandwidth (GHz)	VSWR	Gain (dB)	Directivity (dBi)	Efficiency (%)
26.75	-22.02	0.52	1.17	9.20	9.91	93.00
28.00	-23.14	1.10	1.15	11.39	12.12	94.00

Figure 14(a) presents the S_{11} and bandwidth parameters, while Figure 14(b) illustrates the VSWR. Figures 15(a) and 15(b) show the gain and directivity at 26 GHz, respectively. Similarly, Figures 16(a) and 16(b) depict the gain and directivity at 28 GHz, respectively, for the slotted CSRR-loaded MRPA antenna.

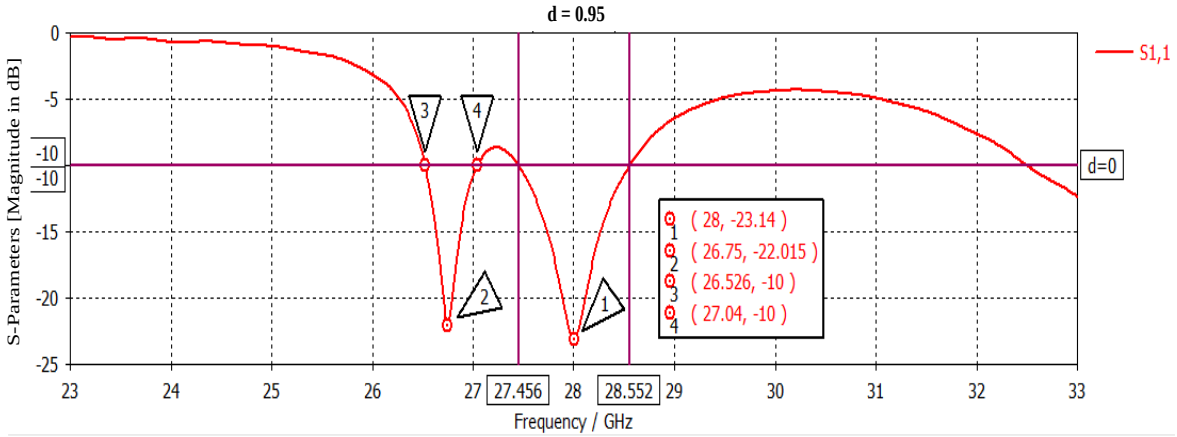

Figure 14 (a): S_{11} and Bandwidth as functions of frequency

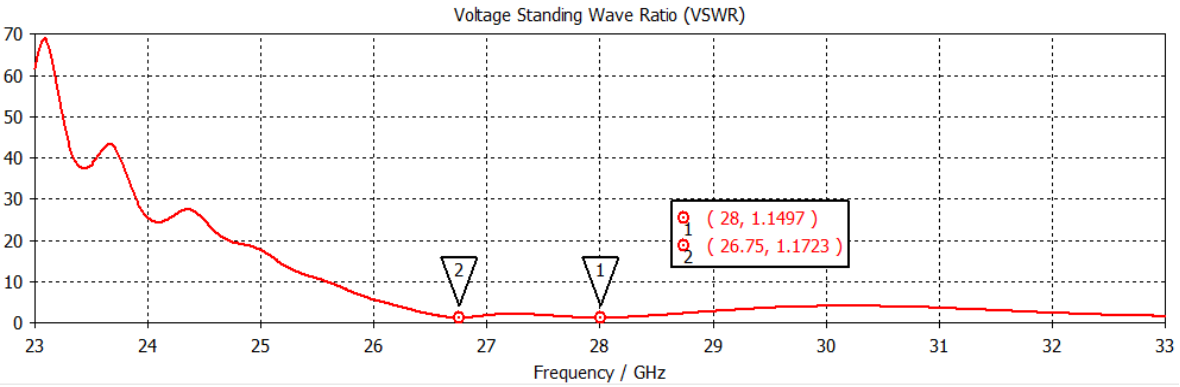

Figure 14(b): VSWR parameter as a function of frequency for the antenna in Figure 5(a-c)

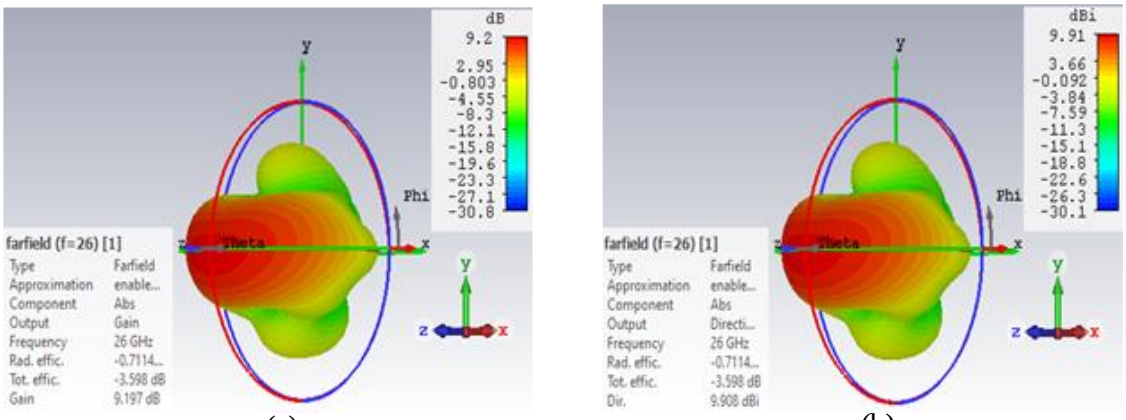

(a) (b)

Figure 15(a)(b): Gain and directivity for the antenna in Figure 5(a-c) at 26 GHz

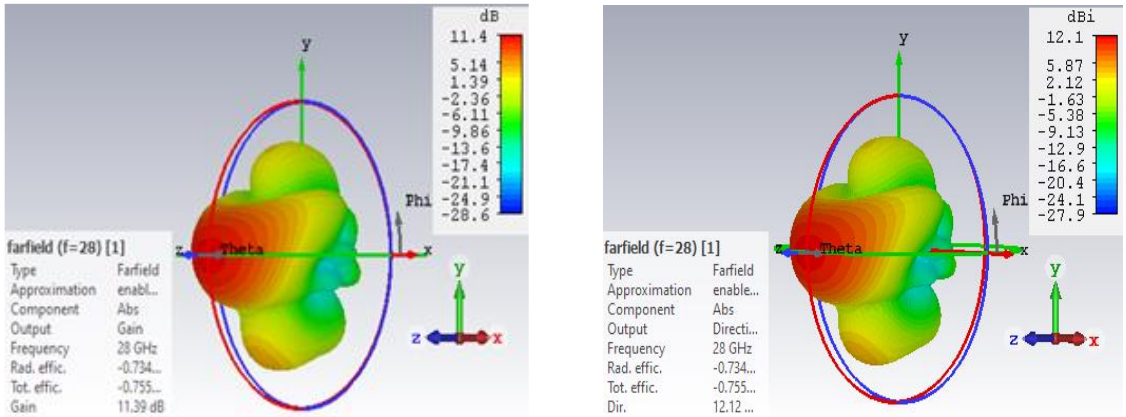

(a) (b)

Figure 16(a)(b): Gain and directivity for the antenna in Figure 5(a-c) at 28 GHz

Table 9: Comparison of conventional MRPA with LIU shape-slotted MRPA with CSRRs

Parameters	**Conventional MRPA**	**LIU shape slotted MRPA with CSRRs**	**Annotation**
Antenna size	16.5x20 (330 mm^2)	15.5x17 (264 mm^2)	Reduction = 20%
Bandwidth at 28 GHz	0.81 GHz	1.16 GHz	Enhancement = 43%
Gain at 28 GHz	9.44 dB	9.95 GHz	Enhancement = 5%

Table 10: Comparison of conventional MRPA with LIL shape slotted MRPA with CSRRs

Parameters	**Conventional MRPA**	**LIL shape slotted MRPA with CSRRs**	**Annotation**
Antenna size	16.5x20 (330 mm^2)	15.5x16 (248 mm^2)	Reduction = 25%
Bandwidth at 26 GHz	0.50 GHz	0.44 GHz	Reduction = 12%
Bandwidth at 28 GHz	0.81 GHz	0.95 GHz	Enhancement = 17%
Gain at 26 GHz	5.81 dB	8.46 dB	Enhancement = 46%
Gain at 28 GHz	9.44 dB	11.19 dB	Enhancement = 19%

Table 11: Comparison of conventional MRPA with LI□ shape-slotted MRPA with CSRR

Parameters	**Conventional MRPA**	**LI□ shape slotted MRPA with CSRRs**	**Annotation**
Antenna size	16.5x20 (330 mm^2)	15.5x16 (248 mm^2)	Reduction = 25%

Bandwidth at 26 GHz	0.50 GHz	0.52 GHz	Enhancement = 4%
Bandwidth at 28 GHz	0.81 GHz	1.10 GHz	Enhancement = 36%
Gain at 26 GHz	5.81 dB	9.20 dB	Enhancement = 58%
Gain at 28 GHz	9.44 dB	11.39 dB	Enhancement = 21%

Table 9-11 compares the conventional MRPA with LIU, LIL, and LI□ shape slotted MRPA antennas loaded with CSRRs regarding size, bandwidth, and gain at the selected frequency bands. The LI□ shape slotted MRPA with CSRRs shows a 25% size reduction and gave the best gain performance, while that with LIU slots gave the best bandwidth.

Table 13: Comparison of our designs with CSRR-Loaded antennas in the 5G Band

References	**Size (mm^2)**	**Frequency (GHz)**	**Minimum S_{11} (dB)**	**BW (GHz)**	**VSWR**	**Gain (dB)**	**Directivity (dBi)**	**Efficiency (%)**
This work	15.5x16	28.00	-23.14	1.10	1.15	11.39	12.12	**94.00**
This work	15.5x16	28.00	-30.66	0.95	1.06	11.19	11.96	**94.00**
This work	15.5x17	28.00	-30.37	1.16	1.06	9.95	11.07	**90.00**
[1]	15x15	28.07	-33.16	2.83	-	6.81	8.15	**71.22**
[11]	12x25.4	28.00	≤ 10	6.30	-	6.40	-	-
[14]	28x28	5.20	-19.19	1.04	-	6.30	-	**91.00**
[22]	45x45	6.18	-28.0	0.42	-	3.16	-	**66.39**
[23]	12x12	3.50	-20.41	0.20	-	-3.70	-	**24.10**

Table 13 provides a comparative examination of our proposed designs against earlier published CSRR-based antennas. This study emphasizes the integration of slots and CSRRs to achieve compact size, wide bandwidth, and high gain for 5G applications. As shown in Table 13, our simulated slotted CSRR-loaded antennas are more compact than most earlier CSRR-based designs, except for [1,23], which operate at lower frequencies and achieve a smaller size at the cost of reduced gain and efficiency. Our designs attain an ultimate bandwidth of 1.16 GHz, a superior gain of 11.39 dB, directivity of 12.12 dBi, and efficiency of 94%, within a compact area. Although [1,11] reported higher bandwidths, their designs compromised size, gain, and efficiency.

5.0 CONCLUSION

We have demonstrated that a compact, bandwidth-enhanced, and high-gain MRPA antenna suitable for 5G mobile communication systems can be realized via slots and CSRR configurations. The primary objective was to minimize antenna size while enhancing bandwidth and gain by integrating slots and CSRRs into the patch and ground planes rather than employing an array configuration. To validate this, we designed and simulated a conventional MRPA antenna and a slotted CSRR-loaded MRPA antenna effective at 26 and 28 GHz using CST Studio Suite 2018. The proposed slotted CSRR-loaded antennas are more compact than most previously studied MIMO and slotted CSRR-based designs, except for [1,23], which achieved a smaller size at the cost of reduced gain and efficiency. Our design in Figure 5(a-c) attains a notable bandwidth of 1.10 GHz and a superior gain of 11.39 *d*B within a compact area of 15.5 × 16 mm². Other radiation parameters, like S_{ll}, VSWR, efficiency, and directivity, also exhibited strong performance. These results indicate that the proposed slotted CSRR-loaded MRPA provides a compact, bandwidth-enhanced, and cost-effective solution for seamless integration into handheld 5G devices, avoiding the increased size and weight associated with array-based designs.

References

[1] M. Singh, S. Singh, and M. Tariqul, "CSRR loaded high gained 28 / 38GHz printed MIMO patch antenna array for 5G millimeter wave wireless devices," *Microelectron. Eng.*, vol. 262, no. 1, p. 111829, 2022, doi: 10.1016/j.mee.2022.111829.

[2] M. S. Haroon *et al.*, "Interference Management in Ultra-Dense 5G Networks with Excessive Drone Usage," *IEEE Access*, vol. 8, pp. 102155–102164, 2020, doi: 10.1109/ACCESS.2020.2998494.

[3] J. Khan, D. A. Sehrai, and U. Ali, "Design of Dual Band 5G Antenna Array with SAR Analysis for Future Mobile Handsets," *J. Electr. Eng. Technol.*, vol. 14, no. 2, pp. 809–816, 2019, doi: 10.1007/s42835-018-00059-9.

[4] J. F. Harvey, M. B. Steer, and T. S. Rappaport, "Exploiting high millimeter wave bands for military communications, applications, and design," *IEEE*

Access, vol. 7, no. X, pp. 52350–52359, 2019, doi: 10.1109/ACCESS.2019.2911675.

[5] M. H. Sharaf, A. I. Zaki, R. K. Hamad, and M. M. M. Oma, "A novel dual-band (38/60 GHz) patch antenna for 5G mobile handsets," *Sensors (Switzerland)*, vol. 20, no. 9, 2020, doi: 10.3390/s20092541.

[6] S. N. Nafea and N. N. Khamiss, "For 5G applications, high-gain patch antenna in Ka-Band," *Indones. J. Electr. Eng. Comput. Sci.*, vol. 31, no. 2, pp. 802–809, 2023, doi: 10.11591/ijeecs.v31.i2.pp802-809.

[7] N. Q. A. Alshaikhli, M. A. Neamah, and M. I. Aal-Nouman, "Design of triband antenna for telecommunications and network applications," *Bull. Electr. Eng. Informatics*, vol. 11, no. 2, pp. 1084–1090, 2022, doi: 10.11591/eei.v11i2.3233.

[8] M. Nahas, "A Super High Gain L-Slotted Microstrip Patch Antenna For 5G Mobile Systems Operating at 26 and," *Eng. Technol. Appl. Sci. Res.*, vol. 12, no. 1, pp. 8053–8057, 2022.

[9] M. Nahas, "Design of a high-gain dual-band LI-slotted microstrip patch antenna for 5G mobile communication systems," *J. Radiat. Res. Appl. Sci.*, vol. 15, no. 4, p. 100483, 2022, doi: 10.1016/j.jrras.2022.100483.

[10] C. Milias *et al.*, "Metamaterial-Inspired Antennas: A Review of the State of the Art and Future Design Challenges," *IEEE Access*, vol. 9, pp. 89846–89865, 2021, doi: 10.1109/ACCESS.2021.3091479.

[11] M. Venkateswara Rao, B. T. P. Madhav, J. Krishna, Y. Usha Devi, T. Anilkumar, and B. Prudhvi Nadh, "CSRR-loaded T-shaped MIMO antenna for 5G cellular networks and vehicular communications," *Int. J. RF Microw. Comput. Eng.*, vol. 29, no. 8, pp. 1–14, 2019, doi: 10.1002/mmce.21799.

[12] S. Didi, I. Halkhams, M. Fattah, Y. Balboul, M. El Bekkali, and S. Didi, "Design of a microstrip antenna patch with a rectangular slot for 5G applications operating at 28 GHz," *TELKOMNIKA Telecommun. Comput. Electron. Control*, vol. 20, no. 3, pp. 527–536, 2022, doi: 10.12928/TELKOMNIKA.v20i3.23159.

[13] S. Rana and M. R. Smieee, "Design and analysis of microstrip patch antenna for 5G wireless communication systems," *Cogent Eng.*, vol. 11, no. 6, pp. 1–15, 2022, doi: 10.11591/eei.v11i6.3955.

[14] M. Shobana, "CSRR-inspired antenna using artificial neural network for sub 6 GHz 5G applications," *Alexandria Eng. J.*, vol. 77, pp. 351–367, 2023, doi: 10.1016/j.aej.2023.06.085.

[15] M. J. R. Kraus, J. D., *Antennas-for-All-Applications*, Sixth. Tata McGraw-Hill Publishing Companies, inc.New York, 1997.

[16] C. A. Balanis, *Antenna Theory: Analysis and Design*, 4th ed. John Wiley & Sons, Inc., Hoboken, New Jersey, Canada., 2016.

[17] L. G. Ayalew and F. M. Asmare, "Design and Optimization of Pi-Slotted Dual-Band Rectangular Microstrip Patch Antenna using Surface Response Methodology for 5G Applications," *Heliyon*, vol. 8, no. August, p. e12030, 2022, doi: 10.1016/j.heliyon.2022.e12030.

[18] M. Aminu-baba *et al.*, "A compact triband miniaturized MIMO antenna for WLAN applications," *AEUE - Int. J. Electron. Commun.*, vol. 136, no. April, p. 153767, 2021, doi: 10.1016/j.aeue.2021.153767.

[19] J. D. Baena *et al.*, "Equivalent-circuit models for split-ring resonators and complementary split-ring resonators coupled to planar transmission lines," *IEEE Trans. Microw. Theory Tech.*, vol. 53, no. 4 II, pp. 1451–1460, 2005, doi: 10.1109/TMTT.2005.845211.

[20] D. M. Pozar, *Microwave Engineering*, Fourth Edi. John Wiley & Sons, Inc., Hoboken, New Jersey, Canada., 2012.

[21] M. A. Yusuf and M. H. Ali, "Design of a High Gain Dual-Band Compact Slotted Microstrip Patch Antenna for 5G Mobile Communication Systems," *BENIN J. Phys. Sci. BJPS*, vol. 1, no. 2, pp. 131–144, 2024.

[22] M. Aminu-Baba *et al.*, "A compact triband microstrip antenna utilizing hexagonal CSRR for wireless communication systems," *Bull. Electr. Eng. Informatics*, vol. 9, no. 5, pp. 1916–1923, 2020, doi: 10.11591/eei.v9i5.2191.

[23] C. Josephine, M. Andrews, A. Santhosh, and K. Narayanan, "Compact Metamaterial based Antenna for 5G Applications," *Results Eng.*, vol. 24, no. October, p. 103269, 2024, doi: 10.1016/j.rineng.2024.103269.